

Privacy-preserving fall detection at the edge using Sony IMX636 event-based vision sensor and Intel Loihi 2 neuromorphic processor

Lyes Khacef*, Philipp Weidel[‡], Susumu Hogyoku[†], Harry Liu[¶], Claire Alexandra Bräuer*, Shunsuke Koshino[†], Takeshi Oyakawa[†], Vincent Parret*, Yoshitaka Miyatani[†], Mike Davies[¶], Mathis Richter[§]

* Sony Advanced Visual Sensing AG, Schlieren, Switzerland

[†] Sony Semiconductor Solutions Corporation, Research Division 1, Tokyo, Japan

[‡] Intel Labs, Intel Semiconductor AG, Zurich, Switzerland

[§] Intel Labs, Intel Deutschland GmbH, Feldkirchen, Germany

[¶] Intel Labs, Intel Corporation, Santa Clara, CA, USA

Abstract—Fall detection for elderly care using non-invasive vision-based systems remains an important yet unsolved problem. Driven by strict privacy requirements, inference must run at the edge of the vision sensor, demanding robust, real-time, and always-on perception under tight hardware constraints. To address these challenges, we propose a neuromorphic fall detection system that integrates the Sony IMX636 event-based vision sensor with the Intel Loihi 2 neuromorphic processor via a dedicated FPGA-based interface, leveraging the sparsity of event data together with near-memory asynchronous processing. Using a newly recorded dataset under diverse environmental conditions, we explore the design space of sparse neural networks deployable on a single Loihi 2 chip and analyze the tradeoffs between detection F_1 score and computational cost. Notably, on the Pareto front, our LIF-based convolutional SNN with graded spikes achieves the highest computational efficiency, reaching a $55\times$ synaptic operations sparsity for an F_1 score of 58%. The LIF with graded spikes shows a gain of 6% in F_1 score with $5\times$ less operations compared to binary spikes. Furthermore, our MCUNet feature extractor with patched inference, combined with the S4D state space model, achieves the highest F_1 score of 84% with a synaptic operations sparsity of $2\times$ and a total power consumption of 90 mW on Loihi 2. Overall, our smart security camera proof-of-concept highlights the potential of integrating neuromorphic sensing and processing for edge AI applications where latency, energy consumption, and privacy are critical.

Index Terms—Edge AI, fall detection, always-on inference, event-based sensing, sparse processing, neuromorphic computing.

I. INTRODUCTION

The world population is rapidly growing with an increase in life expectancy, particularly in developed countries [1]. Consequently, elderly care is a global concern which is gaining attention. In particular, falls are becoming a major public health problem for the elderly [2]. According to the World Health Organization, falls are the second most common cause of unintentional injury-related deaths worldwide, after road traffic accidents [3]. Therefore, there is a growing need for fall detection systems in the healthcare industry. A fall detection system aims to trigger an alert *after* a fall has occurred to emergency caregivers [4]. On the one hand, quick response is

critical after a fall and medical outcomes of falls as well as the associated healthcare expenses largely depend on rescue time [5], [6]. On the other hand, it has been shown that fall detection systems decrease the fear of falling, which in turn can decrease the likelihood of a fall [5], [7].

Fall detection systems use two main types of sensors [8]: body-worn inertial sensors and vision sensors. Accelerometers and gyroscopes embedded in smartphones and smartwatches measure body motion independently of environmental factors (e.g., objects, lighting). However, continuous wear and regular recharging limit their practicality, particularly for elderly people [9]. In contrast, vision sensors like RGB cameras, infrared cameras, depth cameras, and 3D-based methods using camera arrays are non-intrusive for the user and provide continuous passive monitoring without depending on user compliance. They are therefore useful in settings such as nursing homes, hospitals, or assisted living facilities. Combined with deep learning models, vision-based solutions can be highly accurate and adaptable to different environments [10]. Yet, privacy concerns remain substantial [11]–[13] as residents often oppose in-room cameras [14]. Studies on fall detection usually lack strategies to effectively ensure data privacy, which prevents their real-life deployment [12].

In this work, we propose a privacy-preserving vision-based solution that consists of the Sony¹ Event-based Vision Sensor (EVS) [15] which only captures per-pixel changes of light intensity in the form of events, combined with the Intel² Loihi 2 [16] which directly processes these events asynchronously in a fast and efficient way. This system effectively preserves privacy by processing the sparse event stream in real time, enabling rapid detection while ensuring that events are discarded immediately after processing at the edge. In addition, it reduces energy consumption by exploiting the sparsity of input events and neural networks activations which is important for always-on inference, especially when a

¹Sony is a registered trademark of Sony Group Corporation or its affiliates.

²Intel is a registered trademark of Intel Corporation or its affiliates.

battery-powered operation is needed. Beyond the fall detection application, this smart security camera is a proof-of-concept of real-time always-on perception systems at the edge where latency, energy consumption, and privacy matter.

In the last five years, event-based vision sensing has been extensively explored to solve many classes of computer vision problems such as classification, segmentation, detection, and tracking [17]–[21]. However, when targeting a fully embedded system, EVS requires dedicated processing to realize the latency and energy efficiency advantages of the sensor at the system level. In particular, asynchronous near-memory processing using digital neuromorphic chips is a natural fit in terms of processing paradigm and technology maturity to exploit the high temporal resolution and sparsity of event streams [22]–[24]. This end-to-end neuromorphic sensing and processing approach was particularly studied using the Intel Loihi research chip [16], which was shown to be 3-30× more energy-efficient than the embedded Nvidia GPUs [25], [26].

The main limitation of these works is the USB-based interface, which allows for high flexibility but imposes bottlenecks on the speed and efficiency of the system. Therefore, there is growing interest for direct interfaces between EVS and embedded processors. For example, dedicated interfaces have been developed to connect EVS with FPGA-based processing [27]. However, these systems remain power-hungry as they target programmability over efficiency. Other systems in research [28] and industry [29], [30] propose dedicated interfaces on ASICs, but they use low-resolution EVS (typically 128×128 pixels) and embed very constrained processors, limiting the system’s accuracy and robustness for complex computer vision tasks.

This work presents the following key contributions toward a robust, privacy-preserving embedded fall-detection system:

- We present a new FPGA-based interface that directly connects the IMX636 sensor with the Loihi 2 processor.
- Using a newly recorded dataset, we explore and benchmark different algorithmic solutions on a single Loihi 2 chip, evaluating detection F_1 score, latency, computational sparsity/cost, and power consumption.
- We introduce graded spikes for Leaky Integrate-and-Fire (LIF) models and investigate their impact in Spiking Neural Networks (SNNs), achieving the highest sparsity.
- We deploy for the first time an MCUNet architecture on neuromorphic hardware using patched inference to fit in a single Loihi 2 chip. We combine it with a State Space Model (SSM), achieving the highest F_1 score.
- We provide insights into the trade-offs along the Pareto front between F_1 score and computational cost, demonstrating the possibilities of integrating the IMX636 sensor with the Loihi 2 processor.

II. SENSING AND PROCESSING TECHNOLOGIES

We introduce the IMX636 EVS sensor and the Loihi 2 asynchronous processor, which we integrate using a direct FPGA-based interface to realize the low-latency and low-power advantages of EVS at the system level.

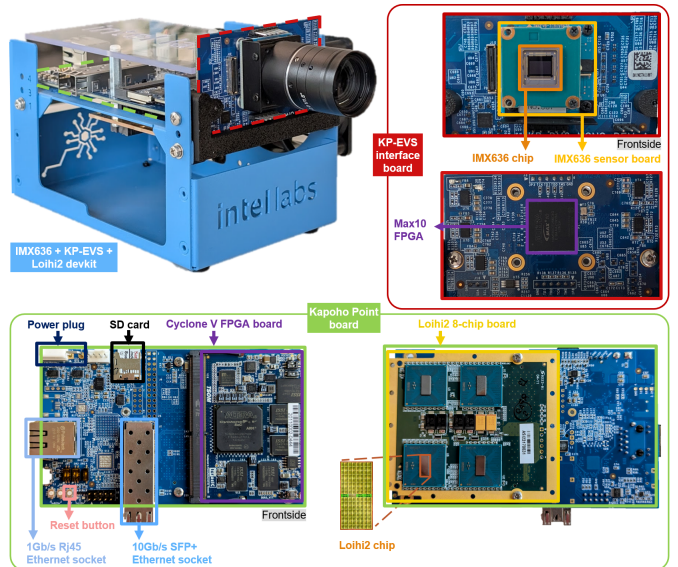


Fig. 1. Hardware system overview showing the whole system (*top left*), the KP-EVS interface board (*top right*), the host board with IO and power interfaces (*bottom left*), and a Kapoho Point (KP) board with 8 Loihi 2 chips (only one chip is used in our work) (*bottom right*).

A. Sony IMX636 sensor

EVS are bio-inspired sensors that asynchronously output per-pixel luminance changes in the form of events. Each pixel independently emits an event when the log-brightness difference since the last event reaches a threshold [17]. An event i is denoted by $e_i = (x_i, y_i, t_i, p_i)$, where x_i and y_i are the pixel coordinates, t_i is the timestamp with μs resolution and $p_i \in \{+, -\}$ is the polarity, i.e., positive or negative for an increase or decrease in light intensity, respectively. This differential sensing paradigm leverages the redundancy in the natural environment, and outputs sparse events with low latency (less than $100 \mu s$ at 1 KLux), high temporal resolution (μs), low power (32 mW at 0.1 M events/s, 73 mW at 300 M events/s) and high dynamic range (beyond 120 dB) [31], [32].

The IMX636 sensor [15] was developed in a collaboration between Sony and Prophesee, combining Sony Semiconductor Solutions’s CMOS image sensor technology with Prophesee’s event-based vision sensing technology. In particular, the light-receiving and luminance detection circuits are incorporated on different layers: a pixel chip with a programmable Region of Interest (ROI), and a logic chip which includes integrated signal processing circuits (e.g., anti-flicker, event filter, and event rate control). These chips are stacked and connected using Cu-Cu technology within each pixel. The IMX636 sensor has an HD resolution of 1280×720 pixels, using the industry’s smallest pixel of $4.86 \mu m$ among stacked EVS, integrated with the logic chip in a 40 nm process [31], [32].

B. Intel Loihi 2 processor

Loihi 2 is the second generation of the Loihi research chip [33], [34], a fully digital asynchronous chip manufactured

using Intel 4 process technology. It uses 128 near-memory asynchronous processing neuro-cores and 2 networks-on-chip for sparse communication among these cores. It also includes 6 embedded, synchronous x86 Lakemont cores for management, such as network configuration and data encoding/decoding. Multiple Loihi 2 chips can be combined to form larger systems; Fig. 1 shows a KP system with 8 Loihi 2 chips.

Loihi 2 uses barrier synchronization between cores to ensure that all neurons compute within the same global algorithmic timestep in a deterministic way [33], [35]. With stored data, the chip operates as fast as possible, whereas with streamed data, the chip can operate based on physical time (using the clock of the x86 cores), event count, or any signal from an external host or device. In addition, algorithmically, Loihi 2 supports sparse (beyond conventional spiking) neural network deployment due to its programmable neuro-core and graded spike message-passing [36]. The Loihi 2 inference can therefore match the accuracy of the same quantized model on an ANN accelerator, while achieving higher computing efficiency by exploiting the unstructured sparsity [37], [38] of synaptic operations (SynOps). Using Loihi 2, we aim not for biological plausibility, but for energy efficiency via biological inspiration.

III. METHODS

This section describes the FPGA-based hardware interface and defines our algorithmic exploration with four neural architectures of less than a million parameters which can be deployed on a single Loihi 2 chip (CNN, MLP, MCUNet, S4D), five neuron models (ReLU, SigmaDelta, binary LIF, graded LIF, SSM), as well as the Loihi 2-aware patched inference and training methods.

A. Dedicated hardware interface

The KP-EVS dedicated hardware interface connects the IMX636 sensor chip to the KP processing system via an interface board (top right of Fig. 1, Fig. 2). The logic is implemented on a Max10 10M50 FPGA from Altera. It accepts EVT3 events from the IMX636 sensor over MIPI CSI-2 (2 lanes at 600 Mbps), applies cropping (drop events outside a rectangular ROI) and down-sampling (reduce spatial resolution), maps each event to an algorithmic timestep and up to 4 neuro cores to spike to, synchronizes with Loihi 2, and forwards the spikes via Parallel Input-Output (PIO) at the required timestep. A Nios II embedded processor core supports management access for configuring event processing and spike generation, and for configuring and controlling the IMX636 sensor through I2C. Validation and visualization is supported by an optional mirroring of received EVT3 events and generated spikes. The full design maps to 17K logical elements and 128 KB of memory, and runs at 100 MHz.

B. Neural network architectures

CNN. We use the following 5-layer Convolutional Neural Network (CNN) topology: $160 \times 160 \times 2 - 16c3 - 32x3 - 64c3 - 128c3 - 256c3$, where XcY denotes a convolution layer

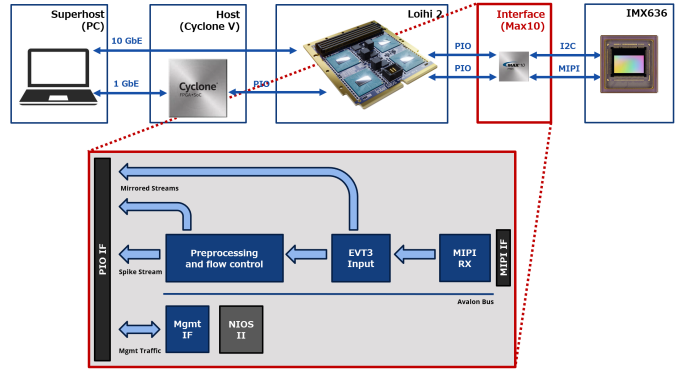


Fig. 2. Hardware system pipeline with details of Max10 FPGA interface.

with X kernels of shape $Y \times Y$. All convolution layers have a stride of 2. The output features have a size of $4 \times 4 \times 256$.

MLP. On top of the CNN and after a flattening layer, a 3-layer Multi-Layer Perceptron (MLP) is used with the following fully-connected topology: $128 - 64 - 2$. Two output neurons are used to represent the classes ‘Fall’ and ‘NoFall’.

MCUNet. MCUNet is a CNN-based model designed to run on tiny hardware resources for always-on inference in IoT devices [39], [40]. It has 18 MobileNet inverted residual blocks [41], characterized by depthwise separable convolution [42], linear bottlenecks, inverted residuals, and non-linear activation. Nevertheless, it is possible to use an arbitrary number of blocks, which is denoted by MCUXB, where X refers to the number of blocks. For instance, we only use 13 blocks to deploy the model on a single Loihi 2 chip. Notably, this is the first time that such a State-Of-The-Art (SOTA) CNN architecture is deployed on neuromorphic hardware.

S4D. On top of the stateless CNN/MCUNet spatial feature extractors and after average pooling and flattening, a State Space Model (SSM) is used for temporal feature extraction. SSMs have recently been positioned as a promising alternative to Transformers for sequence modeling [43]. In their convolutional form, unlike recurrent neural networks, they enable highly parallel training on GPUs with stored data. In their recurrent form, they do not suffer from the quadratic scaling of compute cost of the attention mechanism of Transformers, allowing for linear scaling and efficient inference with streaming data. The S4D model [44] is a variant of the Structured State Space for Sequence Modeling (S4) architecture, where a diagonal state space matrix is used to simplify the kernel computation. It was successfully deployed on Loihi 2 [45].

C. Neuron models

For all neuron models, let us consider the activation z at the algorithmic time step t as follows:

$$z[t] = \sum_{i=1}^n w_i \times x_i[t] + b$$

where w_i and x_i are the weight and the input of the synapse i , respectively, n is the number of synapses, and b is a bias.

Let us also define spiking neurons as stateful neurons with sparse activations in the form of binary or graded (i.e., valued) spikes, including thus SigmaDelta and LIF neurons.

ReLU. ReLU neurons output $y[t]$ is defined as follows:

$$y[t] = \begin{cases} z[t] & \text{if } z[t] \geq 0 \\ 0 & \text{otherwise} \end{cases}$$

It adds non-linearity by zeroing the negative activations, which introduces some inherent sparsity.

SigmaDelta. SigmaDelta neurons aim to further sparsify the ReLU output with the stateful Delta encoder as follows:

$$a[t] = \begin{cases} z[t] & \text{if } z[t] \geq 0 \\ 0 & \text{otherwise} \end{cases}$$

$$\Delta a[t] = a[t] - a[t-1] + r[t-1]$$

$$y[t] = \begin{cases} \Delta a[t] & \text{if } \Delta a[t] \geq \vartheta \\ 0 & \text{otherwise} \end{cases}$$

$$r[t] = \Delta a[t] - y[t]$$

where $a[t]$ is the ReLU output, $r[t]$ is the residual state, $y[t]$ is the output and ϑ is the learnable spike threshold. The Delta encoder sends a graded spike with a value of $y[t]$ when $\Delta a[t]$ exceeds the threshold ϑ , while the Sigma decoder receives the sparse event messages and accumulates them to restore the original information.

LIF with binary/graded spikes. LIF neurons are behavioral models of biological neurons, derived from the spike response model [46]. We use the current-based LIF neuron which is useful for learning patterns with a rich temporal structure [47]. The LIF dynamics are expressed as follows:

$$i[t] = \alpha \times i[t-1] + z[t]$$

$$u[t] = \beta \times u[t-1] \times (1 - \mathcal{H}(u[t-1] - \vartheta)) + i[t]$$

$$y[t] = \begin{cases} u[t] & \text{if } u[t] \geq \vartheta \text{ and } \textit{graded spikes} \\ 1 & \text{if } u[t] \geq \vartheta \text{ and } \textit{binary spikes} \\ 0 & \text{otherwise} \end{cases}$$

where $i[t]$ and $u[t]$ are the current and voltage states respectively, α and β are the current and voltage decays respectively, \mathcal{H} is the Heaviside step function used for the hard reset, ϑ is the learnable spike threshold, and $y[t]$ is the output spike which can be binary or graded depending on the LIF model.

SSM. We implement the SSM neuron model in two different forms, as explained in Sec. III-B. For training, we use the convolutional form of the S4D model allowing parallel and much faster execution on GPUs. For inference, we represent the S4D dynamics in its time-discrete recurrent formalization as follows:

$$s[t] = a \times s[t-1] + b \times z[t]$$

$$y[t] = c \times s[t]$$

where $s[t]$ is the neuron's state, a , b and c are the local parameters and $y[t]$ is the output. In fact, the recurrent weight matrix A , the input projection matrix B , and the output

projection matrix C of the S4D model are diagonalized, so their diagonal values become local dynamical parameters per neuron, analogous to the synaptic and membrane decay factors (or time constants) of LIF neurons [48], [49].

D. Patched inference

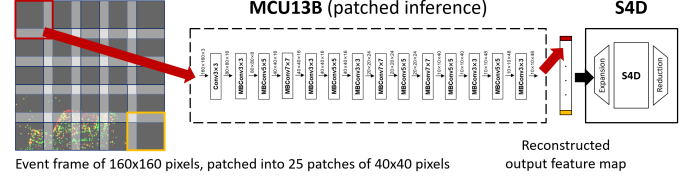


Fig. 3. Input-patched inference of MCU13B model for a single event frame, which reduces the memory requirements by an order of magnitude by reusing the Loihi 2 neuro-core memories for each patch.

Despite using only 13 blocks of MCUNet, we need around 10 Loihi 2 chips to deploy the entire network due to the large feature map sizes (i.e., number of neurons). However, since the model is stateless, there is no need to keep the neurons states for consecutive time steps. Therefore, we adapt and use the patched inference proposed in [40], where the authors split the input into multiple *patches*, and process multiple layers per patch to reduce the peak memory requirement of the model. Similarly, we split the 160x160 pixels input into 25 patches of 40x40 pixels as shown in Fig. 3, with a stride of 30 pixels (i.e., overlap of 10 pixels).

The patches are processed sequentially, where each patch goes through the whole 13 blocks of MCU13B (not just a few layers as in [40]) and only the final output feature map is saved. By reusing the Loihi 2 neuro-core memories for each patch, this input-patched inference drastically reduces the memory requirements by an order of magnitude. Once all the patches are processed, the complete output feature map is reconstructed and the S4D inference is triggered. It is to note that the 10 pixels overlap is not enough to produce algorithmically equivalent feature extraction, and this design choice was motivated by the need to fit the model in a single Loihi 2 chip. It is therefore expected to have some loss in feature map quality and overall detection accuracy.

E. Training

Events encoding. The asynchronous events produced by EVS must be *accumulated* into algorithmic timesteps for inference on Loihi 2 and for training on GPUs. We accumulate events into constant temporal windows (i.e., algorithmic timestep duration) and apply a per-pixel and per-polarity count to get a single graded input spike. The only exception is the binary LIF model where we use binary input spikes (i.e., at least one event was received). During Loihi 2 timestep-based inference, event frames are not built, and events are simply encoded into sparse graded spikes.

We design the fall detection system to operate at a fixed throughput of 16 Hz. Accordingly, we use the maximum timestep duration of 60 ms for the S4D-based models to accommodate the processing latency of the patched MCUNet backbone. For the spike-based models, we use a shorter timestep duration of 20 ms to enable finer-grained temporal processing, while accumulating spikes over three consecutive timesteps to maintain the same detection throughput.

Focal loss. Our fall detection dataset is highly imbalanced (7% of falling actions); therefore, we adopt the Focal Loss (FL) [50] to mitigate class imbalance, defined as follows:

$$\text{FL}(p, y) = \begin{cases} -\alpha(1-p)^\gamma \log(p), & \text{if } \hat{y} = 1, \\ -(1-\alpha)p^\gamma \log(1-p), & \text{otherwise.} \end{cases}$$

where $p \in [0, 1]$ is the model’s estimated probability for the fall class with label $\hat{y} = 1$, $\hat{y} \in \{0, 1\}$ is the ground-truth class label, $\alpha \in [0, 1]$ is the balancing factor to address class imbalance, and $\gamma \geq 0$ is the focusing parameter that reduces the relative loss for well-classified samples.

The model’s estimated probability p is calculated over the sample’s duration based on the sum of output spikes for the spike-based models, whereas it is based on the maximum logit difference the continuous-output models.

Backpropagation. While ReLU- and S4D-based models are trained using standard Backpropagation (BP), LIF and SigmaDelta spiking models require a custom BP to address the non-differentiability limitation of their activation functions [51], [52]. In this work, we use the SLAYER framework [53] for direct training of SNNs, as it is widely used and takes into account the hardware constraints (e.g., weight and state quantization) of the Loihi 2 chip.

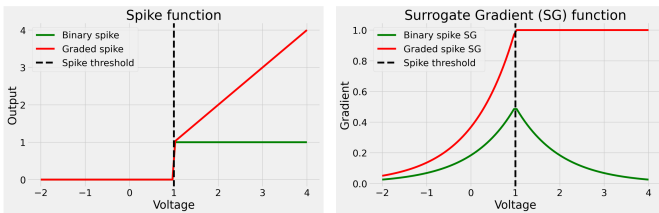


Fig. 4. Spike (activation) functions (*left*) and surrogate gradient functions (*right*) of LIF neurons with binary and graded spikes.

SLAYER is a form of Backpropagation Through Time (BPTT) which uses surrogate gradients in the backward pass [51], as shown in Fig. 4. In addition, gradients are computed jointly in time, reducing the complexity of sequential BPTT by parallelized and GPU-accelerated joint gradient computation [54]. Although it is not mathematically equivalent to BPTT, SLAYER does not differ significantly, in particular when the spiking rate is low.

Hyper-parameters. All models were trained for 100 epochs with a batch size of 16, using $\alpha = 0.9$ and $\gamma = 2.0$ for the

focal loss function. The CNN+MLP models were trained with Quantization-Aware Training (QAT) using 8-bit weights and a learning rate of $1e-5$. The CNN+S4D and MCUNet+S4D were trained with full precision using the convolutional representation of S4D, then quantized and fine-tuned for 10 epochs with QAT using 8-bit weights, a backbone learning rate of $5e-5$ and a S4D learning rate of $5e-6$.

IV. EXPERIMENTS AND RESULTS

In this section, we present our Loihi 2-aware algorithmic exploration and benchmarking with our newly recorded dataset, highlighting the tradeoffs between accuracy and efficiency.

A. Fall detection benchmark

Original dataset. In order to have full control over the environmental conditions, we recorded a new dataset for fall detection, comprising 14 action classes (*falling, seated, standing, sit down, stand up, lying, pick up, touching head, touching back, touching torso, touching neck, coughing, walking, no person*) with about 640 samples (sequences) of 4.6 s per class. In our experiments, we only consider the *falling/no-falling* (imbalanced) binary classification problem.

Dataset recording was performed in 5 locations with different backgrounds (black, white, living room, sun light, water from fountain), light conditions (source, brightness from 10 Lux to 300 Lux), and distance to the camera. Each sample is about 4.6 s long, however we only use the 2 s with most events per sample for training and validation, while we use the full samples for testing. The dataset was split for cross-subject evaluation, with 3906, 3182, 1793 samples for training, validation and test sets, respectively.

In order to deploy the models in a single Loihi 2 chip, we center-cropped the original 1280x720 resolution to 640x640 then downsampled it with 2x2 sum pooling to 160x160. In hardware, the cropping is implemented by defining an ROI on the IMX636 sensor directly, while the downsampling is implemented in the interface board with a simple integer (floor) division by 4 of the x and y coordinates (i.e., keeping the same events throughput). Across the dataset, the class *walking* has the most input events, with an average throughput of 1 million events/s and a peak throughput of 9 million events/s. It is important to note that events timestamps are not used in the real-world inference, however they are still needed to store the dataset and use it in simulation.

Metrics. We follow the benchmarking principles defined in NeuroBench [55], with algorithmic- and system-level evaluations. At the algorithmic level, for a pre-defined throughput of 16 predictions/s, we evaluate in software:

- Detection performance: We evaluate the accuracy, precision, recall and F_1 score. The F_1 score is the most insightful metric due to the fall/no-fall classes imbalance.
- Synaptic operations per second (SynOps/s): We evaluate the number of SynOps/s as a measure of computational cost, and we calculate the SynOps/s sparsity which is the gain (i.e., reduction) compared to an iso-topology neural network with dense processing.

At the system-level using Loihi 2, the F_1 score is the same as in the algorithmic-level evaluation thanks to the Loihi 2-aware modeling and the fully digital and deterministic processing of Loihi 2. Therefore, we evaluate in hardware:

- Latency: We evaluate the input to output latency, i.e., the delay between a given input timestep and the corresponding output after a full neural network inference.
- Number of Loihi 2 cores: It is a measure of the required silicon area, and cannot exceed 128 cores for one chip.
- Power consumption: We measure the static power and the average dynamic power over the test set samples.

B. Algorithmic-level evaluation

The Loihi 2-aware modeling and 8-bit quantization-aware training is performed using LavaDL and NxTorchEV libraries. The results are presented in Tab. I.

Within the CNN+MLP architecture, the ReLU model has the lowest F_1 score of 46.3% due to the stateless processing where only individual event frames are perceived (which can lead to a high recall but very low precision), at the highest cost of 433 M SynOps/s. Using the SigmaDelta model, the F_1 score slightly degrades by 1.4% because even though the model has states, they are used *after* the original ReLU activation to sparsify the activations only without temporal feature extraction, which leads to a SynOps/s decrease of 4.3 \times . Replacing the SigmaDelta by the binary LIF model, the F_1 score increases by 7% thanks to the temporal feature extraction. Computationally, the SynOps/s also increases by 25%, however each SynOp is based on accumulation-only of synaptic weights (i.e., no multiplication) thanks to the binary spike paradigm. Finally, moving from the binary to the graded LIF model, the F_1 score increases by another 6.2% to reach 58.1%, and the SynOps/s decreases by 4.8 \times to 26 M SynOps/s, reaching a overall SynOps/s sparsity of 55.5 \times compared to an iso-topology model with dense processing.

Next, we evaluate the impact of neural network architectures by first using the CNN with ReLU model and replacing the MLP by an S4D layer, decoupling spatial from temporal feature extraction. The F_1 score significantly increases by 18.8% thanks to the temporal feature extraction capabilities of S4D, especially for long-range temporal dependencies, at a cost of 198 M SynOps/s. Second, we replace the CNN by the MCU13B, which improves the F_1 score by another 6.7% thanks to the enhanced spatial feature extraction, with a cost increase of 5.3 \times reaching 1059 M SynOps/s. Notably, the patched inference degrades the F_1 score by about 2%, but allows the model to fit in a single Loihi 2 chip. Overall, as shown in Fig. 5, the two S4D-based models are in the Pareto-front of F_1 score and computational cost, where the MCU13B+S4D is the most accurate, in addition to the graded LIF-based CNN+MLP which is the most compute-efficient.

Fig. 6 shows two samples of fall sequences with sunset (*left*) and fountain (*right*) backgrounds, where the falls are correctly detected *when* they happen using two models. Our qualitative analysis through the test set visualization shows that the NoFall neuron of the CNN+MLP with graded LIFs mainly fires for

sequences with background events or actions with a similarity to falling such as *sit down*, as a way to reduce the probability of false positives. Even though its F_1 score is only 58.1%, the model is able to correctly predict many falls across different light conditions and distance to the camera, as well as when the person is partially occluded. The MCU13B+S4D clearly outperforms it in recall under extreme low light, especially when the person is far and/or highly occluded. The precision of both models is degraded to varying extents due to false positives caused by actions with similar movements to falling, such as *pickup*, *sit down*, and *lying*.

C. System-level evaluation

The Loihi 2 deployment and inference was performed on a KP revision C2 board with a N3C1 Loihi2 chip, using the NxKernel 0.2.1 library. We mapped every model trying to minimize the number of Loihi 2 cores, and we verified that the KP-EVS hardware is electrically functional with an event stream passing through the interface into Loihi 2. However, it was not used in the system-level evaluation which is based on stored data, sending recorded events from the superhost PC to the KP board using the 10G Ethernet interface.

Latency. First, we need to define the two processing schemes of Loihi 2 [45]: (1) *pipelined* processing where each layer is processed once at each hardware timestep, and (2) *fall-through* processing where the input goes through all the layers first in multiple hardware timesteps before moving to the next input. For the CNN-based models with input-parallel processing, a fall-through processing is used and a maximum throughput of 500 hz can be achieved, with a minimum input-output latency of 2 ms. For the MCUN13B+S4D model with input-patched processing, a pipelined processing of the MCU13B backbone is used with 38 hardware steps (13 blocks + 25 input patches), followed by a fall-through processing of the S4D blocks and output linear layers. A maximum throughput of 25 Hz can be achieved with a minimum input-output latency of 40 ms. Therefore, all models are deployed in a single Loihi 2 chip and satisfy their real-time constraints by effectively reaching (and exceeding) the target 16 predictions/s. In the real-world inference, the Loihi 2 chip is slowed-down to operate in real-time, with an input-output latency of 60 ms which is negligible for the fall detection application that does not require a lower latency response.

Power consumption. Tab. II summarizes the Loihi 2 cores usage and power consumption measurements of the three Pareto-front models from our algorithmic-level evaluation. The static power is roughly proportional to the number of used cores, with about 0.75-0.95 mW/core depending on the used resources. Dynamic power is about 8-12 pW/(SynOp/s) (when normalized with the SynOps/s cost from Tab. I), showing that dynamic energy consumption is indeed proportional to the number of SynOps thanks to the asynchronous processing of Loihi 2. Nevertheless, static power is dominant, which reduces the computational efficiency impact of the CNN+MLP with graded LIFs (46.3 mW for 26 M SynOps/s) compared to the MCU13B+S4D (88.9 mW for 1059 M SynOps/s).

TABLE I
ALGORITHMIC-LEVEL EVALUATION RESULTS.

Network architecture	Neuron model	Test performance				SynOps/s	
		Accuracy (%) \uparrow	Precision (%) \uparrow	Recall (%) \uparrow	F_1 score (%) \uparrow	Cost (M/s) \downarrow	Sparsity (x) \uparrow
CNN + MLP	ReLU	86.8 ± 0.2	32.4 ± 0.5	81.0 ± 1.4	46.3 ± 0.7	433	3.3
	SigmaDelta	88.5 ± 0.4	33.9 ± 1.4	66.4 ± 3.2	44.9 ± 2.0	100	14.5
	Binary LIF	90.8 ± 0.3	41.0 ± 1.1	70.4 ± 1.8	51.9 ± 1.4	125	11.6
	Graded LIF	94.4 ± 0.1	61.6 ± 1.3	54.6 ± 1.0	58.1 ± 1.2	26	55.5
CNN + S4D	ReLU + SSM	96.9 ± 0.1	81.8 ± 1.0	72.5 ± 0.9	76.9 ± 0.9	198	2.9
MCU13B + S4D	ReLU + SSM	97.8 ± 0.1	87.1 ± 0.1	80.4 ± 0.5	83.6 ± 0.3	1059	2

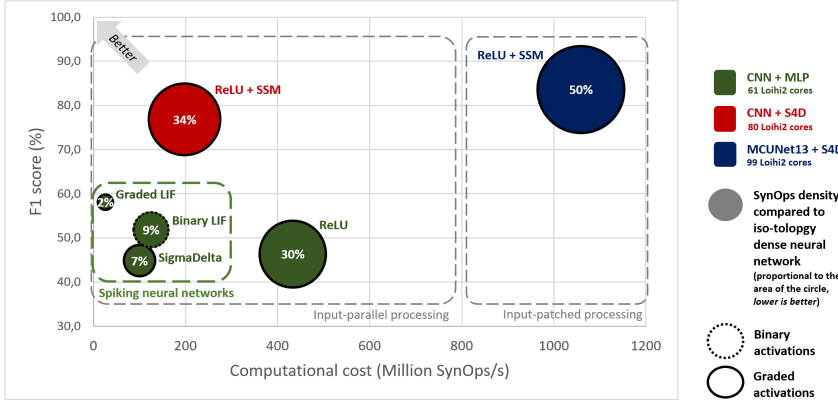


Fig. 5. Fall detection algorithmic-level benchmarking at 16 predictions/s of single Loihi 2 chip compatible models, highlighting the tradeoffs between F_1 score and computational cost.

TABLE II
SYSTEM-LEVEL BENCHMARKING RESULTS OF THE ALGORITHMIC-LEVEL PARETO-FRONT SOLUTIONS.

Pareto front model	Loihi 2 cores	Power (mW)		
		Static	Dynamic	Total
CNN + MLP [Graded LIF]	61	46.0	0.3	46.3
CNN + S4D	80	76.0	1.5	77.5
MCU13B + S4D	99	80.7	8.2	88.9

V. DISCUSSION

A. Improving fall detection F_1 score

Sec. IV-B shows that the biggest improvements in F_1 score come from the neural network architectural changes, with the best F_1 score using MCU13B+S4D which decouples stateless spatial and stateful temporal feature extraction. Notably, this is the first time that such a SOTA architecture is deployed on neuromorphic hardware, thanks to the neuro-cores programmability and graded spike message-passing of Loihi 2.

To explore the potential of the MCUNet feature extractor, we train the full MCU18B+S4D without patching (i.e., cannot be deployed in a single Loihi 2 chip) and reach an F_1 score of 91%, which is a significant improvement of 7.4% with the additional 5 blocks. In order to deploy the model in a single chip, we first need to adapt the MCU18B architecture because of the feature map size becoming smaller than the kernel size after the 13th block when using the current patched inference.

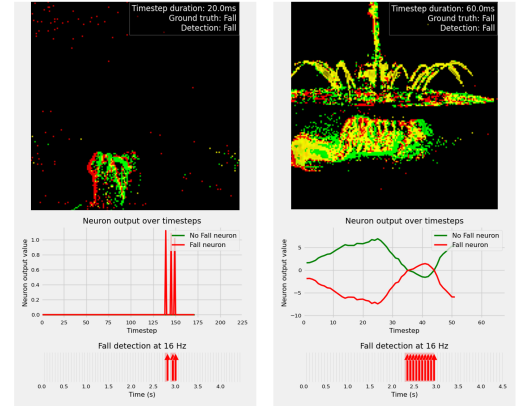


Fig. 6. Events at 3.4s, logits and detection of CNN+MLP with graded LIF (left) and MCU13B+S4D (right).

Then, more resources per core and/or more cores per chip may be needed to embed the full model in a single Loihi 2 chip.

While further algorithmic improvements are likely necessary, a promising approach involves learning the variance of predictions in a self-supervised way. This enables the modeling of input-dependent aleatoric uncertainty [56], which can encourage more robust and reliable predictions [57].

B. Reducing power consumption

First, at the hardware level, the Loihi 2 power consumption is dominated by static power which is due to leakage current, as described in Sec. IV-C. In order to reduce it, a product version of the current Loihi 2 research chip could remove the unused components for a dedicated inference chip, and be manufactured using a more advanced technology process. Once static power is reduced, dynamic power will become more impactful and reducing it will require a higher sparsity of SynOps/s. Loihi 2 can exploit three levels of unstructured sparsity: (1) input event sparsity, which is inherent in EVS and can be improved by adapting the sensor biases, (2) neural network connection sparsity by pruning low-weight/impact synapses and dead neurons which was not explored in this work, and (3) neural activation sparsity which we focused on in this work, however without explicit regularization.

Second, at the algorithmic level, we have seen that activation sparsity is the highest for *stateful* spiking neurons, where the state is either used specifically to sparsify activations as in SigmaDelta neurons, or to further add temporal feature

extraction as in LIF neurons. Stateful models are the most promising for achieving the highest sparsity while maintaining a high accuracy because they can exploit the context encoded in the states [37], at the cost of a higher memory footprint. While stateful processing cannot be applied to the patched MCU13B since Loihi 2 memories are overwritten for each patch, it can be applied to the CNN+S4D model where a variant of the SigmaDelta neuron can be used to sparsify the SSM neurons activations.

Third and finally, the current system is a proof-of-concept with an FPGA-based interface that can be integrated in the next Loihi silicon for a smaller and more efficient two-chip solution. Looking forward, integrating the IMX636 sensor and Loihi 2 processor into a one-chip solution would reduce system footprint while enabling ultra-low latency feedback to the sensor, opening possibilities for scene-specific adaptive sensor control and power optimization. However, such on-sensor integration imposes stringent memory constraints, likely requiring new designs to keep the total on-chip memory within a few hundred kilobytes for small sensors and potentially under one megabyte for larger sensors. These trade-offs will be critical considerations in evolving toward fully integrated neuromorphic vision systems.

C. On-chip anonymization of EVS data

Fully embedded processing is necessary for privacy-preserving fall detection, but it may not be sufficient at the application level as some EVS data may have to be sent to a cloud service in the case of a fall detection, for example, to confirm the need for medical assistance. However, raw events should not be transmitted, because even without full RGB content they can be used to reconstruct grayscale frames, which undermines privacy protection. [58]–[60]. Therefore, on-chip anonymization of the event data that would be transferred (e.g., a sliding-window buffer of a few seconds) is required in an always-on fashion, in parallel to the fall detection inference.

For example, authors in [61] try to anonymize event streams to protect the identity of human subjects against image reconstruction, by scrambling events and enforcing the degradation of such images. However, deploying a similar algorithm in any embedded device remains challenging in terms of required computing resources and power. Further research is required to get a fully privacy-preserving ecosystem which will enable the adoption of security cameras in sensitive environments, using neuromorphic sensing and processing in particular.

VI. CONCLUSION

We presented in this paper a fully embedded system that integrates the Sony IMX636 EVS sensor with the Loihi 2 neuromorphic processor via a dedicated FPGA-based interface. We extensively explored the design space of compatible neural network architectures and neuron models with a thorough benchmarking to understand the tradeoffs between F_1 score and computational cost/energy consumption, and highlighted the most promising models in the Pareto front.

We showed that the proposed graded spikes in LIF models increase the F_1 score by 6.2% and decrease the number of SynOps/s by $4.8\times$ compared to binary spikes, reaching an overall SynOps/s sparsity of $55.5\times$ compared to an isotopology neural network with dense processing. Compared to the binary LIF, the graded LIF comes at the cost of an extra multiplication for each SynOp which is nevertheless natively supported by Loihi 2 thanks to its programmable neuro-core [36]. In addition, it was shown that the main advantage of SNN over ANN accelerators comes from exploiting the sparsity of spikes and not from the replacement of MAC by AC operations [62]. Moving forward, graded spikes can expand the design space of neuromorphic computing algorithms beyond binary SNNs toward a broader category of *sparse neural networks*, including but not limited to graded LIF and SigmaDelta neurons. Further research on hardware and algorithms is required to explore this new paradigm of graded spikes, which can also refine the current abstraction level from biological neurons, moving beyond the binary spike representation to focus on sparsity.

Furthermore, we showed for the first time that we can deploy a SOTA MCU13B spatial feature extractor on neuromorphic hardware, using patched inference to fit the model in a single Loihi 2 chip. Coupled with the S4D temporal feature extractor, the model achieves the highest F_1 score of 83.6 %, satisfies our real-time constraint with 16 predictions/s and only consumes 90 mW on Loihi 2. Nevertheless, about 90% of the total power is static power, which is the main limitation of the hardware system. Such static power can be reduced by removing unused components and manufacturing the next version of the Loihi chip with a more advanced technology process. Our system serves as a proof-of-concept demonstrating the potential of embedding dedicated processing at the edge of EVS via a direct interface, in which events are encoded as graded spikes and processed directly to fully leverage their spatio-temporal sparsity. This approach enables low-latency and low-power perception at the system level.

Beyond the privacy-preserving aspect of edge computing, the always-on perception serves as a filter of raw sensory data by only sending out some data when a pattern of interest is detected (i.e., something *relevant* happens). This drastically reduces the amount of data that need to be transferred, processed and stored in the cloud and thus reduces the overall energy consumption of the application ecosystem. Neuromorphic technologies can enable this transition from cloud-centric to edge-distributed real-time processing toward a more balanced, efficient and scalable ecosystem, while leveraging the growth of IoT and edge sensing markets [63], [64]. By starting from the application requirements and applying a system-level optimization through coherent sensor–processor–algorithm co-development, this work demonstrates a concrete step toward bringing neuromorphic technologies into the real world.

ACKNOWLEDGMENT

We thank Federico Paredes-Vallés, Kirk Scheper, and Sumit Bam Shrestha for their valuable feedback and support.

REFERENCES

- [1] D. Bloom and D. Luca, "Chapter 1 - the global demography of aging: Facts, explanations, future," ser. Handbook of the Economics of Population Aging, J. Piggott and A. Woodland, Eds. North-Holland, 2016, vol. 1, pp. 3–56. [Online]. Available: <https://www.sciencedirect.com/science/article/pii/S2212007616300062>
- [2] N. T. Newaz and E. Hanada, "The methods of fall detection: A literature review," *Sensors*, vol. 23, no. 11, 2023. [Online]. Available: <https://www.mdpi.com/1424-8220/23/11/5212>
- [3] "Falls," *World Health Organization*, 2021. [Online]. Available: <https://www.who.int/news-room/fact-sheets/detail/falls>
- [4] X. Wang, J. Ellul, and G. Azzopardi, "Elderly fall detection systems: A literature survey," *Frontiers in Robotics and AI*, vol. Volume 7 - 2020, 2020. [Online]. Available: <https://www.frontiersin.org/journals/robotics-and-ai/articles/10.3389/frobt.2020.00071>
- [5] M. Mubashir, L. Shao, and L. Seed, "A survey on fall detection: Principles and approaches," *Neurocomputing*, vol. 100, pp. 144–152, 2013, special issue: Behaviours in video. [Online]. Available: <https://www.sciencedirect.com/science/article/pii/S0925231212003153>
- [6] S. K. Gharghan and H. A. Hashim, "A comprehensive review of elderly fall detection using wireless communication and artificial intelligence techniques," *Measurement*, vol. 226, p. 114186, 2024. [Online]. Available: <https://www.sciencedirect.com/science/article/pii/S0263224124000708>
- [7] S. M. Friedman, B. Munoz, S. K. West, G. S. Rubin, and L. P. Fried, "Falls and fear of falling: Which comes first? a longitudinal prediction model suggests strategies for primary and secondary prevention," *Journal of the American Geriatrics Society*, vol. 50, no. 8, pp. 1329–1335, 2002. [Online]. Available: <https://agsjournals.onlinelibrary.wiley.com/doi/abs/10.1046/j.1532-5415.2002.50352.x>
- [8] C. Chen, R. Jafari, and N. Kehtarnavaz, "A survey of depth and inertial sensor fusion for human action recognition," *Multimedia Tools and Applications*, vol. 76, 02 2017.
- [9] E. Alam, A. Sufian, P. Dutta, and M. Leo, "Vision-based human fall detection systems using deep learning: A review," *Computers in Biology and Medicine*, vol. 146, p. 105626, 2022. [Online]. Available: <https://www.sciencedirect.com/science/article/pii/S0010482522004188>
- [10] A. Shojaei-Hashemi, P. Nasiopoulos, J. J. Little, and M. T. Pourazad, "Video-based human fall detection in smart homes using deep learning," in *2018 IEEE International Symposium on Circuits and Systems (ISCAS)*, 2018, pp. 1–5.
- [11] D. N. Serpanos and A. Papalambrou, "Security and privacy in distributed smart cameras," *Proceedings of the IEEE*, vol. 96, no. 10, pp. 1678–1687, 2008.
- [12] R. Igual, C. Medrano, and I. Plaza, "Challenges, issues and trends in fall detection systems," *Biomedical engineering online*, vol. 12, p. 66, 07 2013.
- [13] S. S. Prasad, N. K. Mehta, H. Kumar, A. Banerjee, S. Saurav, and S. Singh, "Hybrid snn-based privacy-preserving fall detection using neuromorphic sensors," in *Proceedings of the Fourteenth Indian Conference on Computer Vision, Graphics and Image Processing*, ser. ICVGIP '23. New York, NY, USA: Association for Computing Machinery, 2024. [Online]. Available: <https://doi.org/10.1145/3627631.3627650>
- [14] T. Xu, Y. Zhou, and J. Zhu, "New advances and challenges of fall detection systems: A survey," *Applied Sciences*, vol. 8, no. 3, 2018. [Online]. Available: <https://www.mdpi.com/2076-3417/8/3/418>
- [15] T. Finateu, A. Niwa, D. Matolin, K. Tsuchimoto, A. Mascheroni, E. Reynaud, P. Mostafalu, F. Brady, L. Chotard, F. LeGoff, H. Takahashi, H. Wakabayashi, Y. Oike, and C. Posch, "5.10 a 1280x720 back-illuminated stacked temporal contrast event-based vision sensor with 4.86µm pixels, 1.066geps readout, programmable event-rate controller and compressive data-formatting pipeline," in *2020 IEEE International Solid-State Circuits Conference - (ISSCC)*, 2020, pp. 112–114.
- [16] M. Davies, A. Wild, G. Orchard, Y. Sandamirskaya, G. Fonseca Guerra, P. Joshi, P. Plank, and S. Risbud, "Advancing neuromorphic computing with loihi: A survey of results and outlook," *Proceedings of the IEEE*, vol. PP, pp. 1–24, 04 2021.
- [17] G. Gallego, T. Delbrück, G. Orchard, C. Bartolozzi, B. Taba, A. Censi, S. Leutenegger, A. J. Davison, J. Conradt, K. Daniilidis, and D. Scaramuzza, "Event-based vision: A survey," *IEEE Trans. Pattern Anal. Mach. Intell.*, vol. 44, no. 1, p. 154–180, Jan. 2022. [Online]. Available: <https://doi.org/10.1109/TPAMI.2020.3008413>
- [18] L. Cordone, B. Miramond, and P. Thierion, "Object detection with spiking neural networks on automotive event data," in *2022 International Joint Conference on Neural Networks (IJCNN)*, 2022, pp. 1–8.
- [19] D. Cazzato and F. Bono, "An application-driven survey on event-based neuromorphic computer vision," *Information*, vol. 15, no. 8, 2024. [Online]. Available: <https://www.mdpi.com/2078-2489/15/8/472>
- [20] Q. Chen, C. Gao, M. Liu, D. Perrone, Y. R. Pei, Z. Wang, Z. Zou, S. Tan, T. Han, G. Lu, Z. Xu, J. Ding, Z. Wang, Z. Wu, H. Han, Y. Wu, J. Chen, W. Zhai, Y. Cao, Z.-j. Zha, N. Bandara, T. Kandappu, A. Misra, X. Lin, H. Huang, H. Ren, B. Cheng, H. M. Truong, V.-T. Ly, H. G. Tran, T.-P. Nguyen, and T. T. Doan, "Event-based eye tracking. 2025 event-based vision workshop," in *2025 IEEE/CVF Conference on Computer Vision and Pattern Recognition Workshops (CVPRW)*, 2025, pp. 5164–5176.
- [21] S. Yang, S. Lu, S. Wang, M. H. Er, Z. Zheng, and A. C. Kot, "Temporal-guided spiking neural networks for event-based human action recognition," 2025. [Online]. Available: <https://arxiv.org/abs/2503.17132>
- [22] D. V. Christensen, R. Dittmann, B. Linares-Barranco, A. Sebastian, M. Le Gallo, A. Redaelli, S. Slesazek, T. Mikolajick, S. Spiga, S. Menzel, I. Valov, G. Milano, C. Ricciardi, S.-J. Liang, F. Miao, A. Mizrahi, P. Yao, J. J. Yang, G. Indiveri, J. P. Strachan, S. Datta, E. Vianello, A. Valentian, J. Feldmann, X. Li, W. H. P. Pernice, H. Bhaskaran, S. Furber, E. Neftci, F. Scherr, W. Maass, S. Ramaswamy, J. Tapson, P. Panda, Y. Kim, G. Tanaka, S. Thorpe, C. Bartolozzi, T. A. Cleland, C. Posch, S. Liu, G. Panuccio, M. Mahmud, A. N. Mazumder, M. Hosseini, T. Mohsenin, E. Donati, S. Tolu, R. Galeazzi, M. E. Christensen, S. Holm, D. Ielmini, and N. Pridys, "2022 roadmap on neuromorphic computing and engineering," *Neuromorphic Computing and Engineering*, vol. 2, no. 2, p. 022501, may 2022. [Online]. Available: <https://doi.org/10.1088/2634-4386/ac4a83>
- [23] C. Schuman, S. Kulkarni, M. Parsa, J. Mitchell, P. Date, and B. Kay, "Opportunities for neuromorphic computing algorithms and applications," *Nature Computational Science*, vol. 2, pp. 10–19, 01 2022.
- [24] D. Kudithipudi, C. Schuman, C. Vineyard, T. Pandit, C. Merkel, R. Kubendran, J. Aimone, G. Orchard, C. Mayr, R. Benosman, J. Hays, C. Young, C. Bartolozzi, A. Majumdar, S. Cardwell, M. Payvand, S. Buckley, S. Kulkarni, H. Gonzalez, and S. Furber, "Neuromorphic computing at scale," *Nature*, vol. 637, pp. 801–812, 01 2025.
- [25] F. Paredes-Vallés, J. J. Hagenars, J. Dupeyroux, S. Stroobants, Y. Xu, and G. C. H. E. de Croon, "Fully neuromorphic vision and control for autonomous drone flight," *Science Robotics*, vol. 9, no. 90, p. eadi0591, 2024. [Online]. Available: <https://www.science.org/doi/abs/10.1126/scirobotics.adi0591>
- [26] E. Ceolini, C. Frenkel, S. B. Shrestha, G. Taverni, L. Khacef, M. Payvand, and E. Donati, "Hand-gesture recognition based on emg and event-based camera sensor fusion: A benchmark in neuromorphic computing," *Frontiers in Neuroscience*, vol. Volume 14 - 2020, 2020. [Online]. Available: <https://www.frontiersin.org/journals/neuroscience/articles/10.3389/fnins.2020.00637>
- [27] P. Bonazzi, C. Vogt, M. Jost, L. Khacef, F. Paredes-Valles, and M. Magno, "Towards low-latency event-based obstacle avoidance on a fpga-drone," in *Proceedings of the IEEE/CVF Conference on Computer Vision and Pattern Recognition (CVPR) Workshops*, June 2025, pp. 4947–4955.
- [28] G. Rutishauser, R. Hunziker, A. Di Mauro, S. Bian, L. Benini, and M. Magno, "Colibries: A milliwatts risc-v based embedded system leveraging neuromorphic and neural networks hardware accelerators for low-latency closed-loop control applications," in *2023 IEEE International Symposium on Circuits and Systems (ISCAS)*, 2023, pp. 1–5.
- [29] M. Yao, O. Richter, G. Zhao, N. Qiao, Y. Xing, W. Dingheng, T. Hu, W. Fang, T. Demirci, M. Marchi, T. Yan, C. Nielsen, S. Sheik, C. Wu, Y. Tian, B. Xu, and G. Li, "Spike-based dynamic computing with asynchronous sensing-computing neuromorphic chip," *Nature Communications*, vol. 15, 05 2024.
- [30] C. Caccavella, F. Paredes-Vallés, M. Cannici, and L. Khacef, "Low-power event-based face detection with asynchronous neuromorphic hardware," in *2024 International Joint Conference on Neural Networks (IJCNN)*, 2024, pp. 1–10.
- [31] S. S. S. Corporation, "Event-based vision sensor (evs)." [Online]. Available: <https://www.sony-semicon.com/en/products/is/industry/evs.html>
- [32] Prophesee, "Stacked event-based vision sensor with the industry's smallest pixels." [Online]. Available: <https://www.prophesee.ai/2020/02/19/prophesee-sony-stacked-event-based-vision-sensor/>

- [33] M. Davies, N. Srinivasa, T.-H. Lin, G. China, Y. Cao, S. H. Choday, G. Dimou, P. Joshi, N. Imam, S. Jain, Y. Liao, C.-K. Lin, A. Lines, R. Liu, D. Mathaikutty, S. McCoy, A. Paul, J. Tse, G. Venkataramanan, Y.-H. Weng, A. Wild, Y. Yang, and H. Wang, "Loihi: A neuromorphic manycore processor with on-chip learning," *IEEE Micro*, vol. 38, no. 1, pp. 82–99, 2018.
- [34] I. N. C. Lab, "Loihi 2 technology brief." [Online]. Available: <https://www.intel.com/content/www/us/en/research/neuromorphic-computing-loihi-2-technology-brief.html>
- [35] C. Li, N. Imam, and R. Manohar, "A deterministic neuromorphic architecture with scalable time synchronization," *Nature Communications*, vol. 16, no. 1, p. 10329, 2025. [Online]. Available: <https://doi.org/10.1038/s41467-025-65268-z>
- [36] S. B. Shrestha, J. Timcheck, E. P. Frady, L. Campos-Macias, and M. Davies, "Efficient video and audio processing with loihi 2," in *ICASSP*, 2024, pp. 13481–13485. [Online]. Available: <https://doi.org/10.1109/ICASSP48485.2024.10448003>
- [37] S. Zhou, C. Gao, T. Delbruck, M. Verhelst, and S. Liu, "Exploiting neuro-inspired dynamic sparsity for energy-efficient intelligent perception," *Nature Communications*, vol. 16, no. 1, p. 9928, 2025. [Online]. Available: <https://doi.org/10.1038/s41467-025-65387-7>
- [38] J. Yik, W. G. Gomez, A. Cheng, B. Leto, A. Pierro, N. Pacik-Nelson, K. V. den Berghe, V. Fra, A. Danielescu, G. Urgese, and V. J. Reddi, "Modeling and optimizing performance bottlenecks for neuromorphic accelerators," 2025. [Online]. Available: <https://arxiv.org/abs/2511.21549>
- [39] J. Lin, W.-M. Chen, Y. Lin, C. Gan, and S. Han, "Mcnunet: Tiny deep learning on iot devices," *Advances in Neural Information Processing Systems*, vol. 33, 2020.
- [40] J. Lin, W.-M. Chen, H. Cai, C. Gan, and S. Han, "Mcnunetv2: Memory-efficient patch-based inference for tiny deep learning," in *Annual Conference on Neural Information Processing Systems (NeurIPS)*, 2021.
- [41] M. Sandler, A. Howard, M. Zhu, A. Zhmoginov, and L.-C. Chen, "Mobilenetv2: Inverted residuals and linear bottlenecks," in *Proceedings of the IEEE Conference on Computer Vision and Pattern Recognition (CVPR)*, June 2018.
- [42] A. Brito, T. Yamasaki, U. Rancon, T. Masquelier, B. R. Cottareau, A. T. Do, and B. Wang, "A 23.5 tops/w depthwise separable convolution accelerator for event-based depth estimation," in *2025 IEEE International Symposium on Circuits and Systems (ISCAS)*, 2025, pp. 1–5.
- [43] B. N. Patro and V. S. Agneeswaran, "Mamba-360: Survey of state space models as transformer alternative for long sequence modelling: Methods, applications, and challenges," *Engineering Applications of Artificial Intelligence*, vol. 159, p. 111279, 2025. [Online]. Available: <https://www.sciencedirect.com/science/article/pii/S0952197625012801>
- [44] A. Gu, A. Gupta, K. Goel, and C. Ré, "On the parameterization and initialization of diagonal state space models," in *Proceedings of the 36th International Conference on Neural Information Processing Systems*, ser. NIPS '22. Red Hook, NY, USA: Curran Associates Inc., 2022.
- [45] S. M. Meyer, P. Weidel, P. Plank, L. Campos-Macias, S. B. Shrestha, P. Stratmann, and M. Richter, "A diagonal structured state space model on loihi 2 for efficient streaming sequence processing," 2024. [Online]. Available: <https://arxiv.org/abs/2409.15022>
- [46] W. Gerstner and W. M. Kistler, *Spiking neuron models: Single neurons, populations, plasticity*. Cambridge university press, 2002.
- [47] M. S. Bouanane, D. Cherifi, E. Chicca, and L. Khacef, "Impact of spiking neurons leakages and network recurrences on event-based spatio-temporal pattern recognition," *Frontiers in Neuroscience*, vol. Volume 17 - 2023, 2023. [Online]. Available: <https://www.frontiersin.org/journals/neuroscience/articles/10.3389/fnins.2023.1244675>
- [48] M. Bal and A. Sengupta, "P-spikessm: Harnessing probabilistic spiking state space models for long-range dependency tasks," in *The Thirteenth International Conference on Learning Representations*, 2025. [Online]. Available: <https://openreview.net/forum?id=Sf4ep9Udjf>
- [49] M. Fabre, L. Dudchenko, and E. Neftci, "Structured state space model dynamics and parametrization for spiking neural networks," 2025. [Online]. Available: <https://arxiv.org/abs/2506.06374>
- [50] T.-Y. Lin, P. Goyal, R. Girshick, K. He, and P. Dollár, "Focal loss for dense object detection," *IEEE Transactions on Pattern Analysis and Machine Intelligence*, vol. 42, no. 2, pp. 318–327, 2020.
- [51] E. O. Neftci, H. Mostafa, and F. Zenke, "Surrogate gradient learning in spiking neural networks: Bringing the power of gradient-based optimization to spiking neural networks," *IEEE Signal Processing Magazine*, vol. 36, no. 6, pp. 51–63, 2019.
- [52] J. K. Eshraghian, M. Ward, E. O. Neftci, X. Wang, G. Lenz, G. Dwivedi, M. Bennamoun, D. S. Jeong, and W. D. Lu, "Training spiking neural networks using lessons from deep learning," *Proceedings of the IEEE*, vol. 111, no. 9, pp. 1016–1054, 2023.
- [53] S. B. Shrestha and G. Orchard, "Slayer: Spike layer error reassignment in time," in *Advances in Neural Information Processing Systems*, S. Bengio, H. Wallach, H. Larochelle, K. Grauman, N. Cesa-Bianchi, and R. Garnett, Eds., vol. 31. Curran Associates, Inc., 2018. [Online]. Available: https://proceedings.neurips.cc/paper_files/paper/2018/file/82f2b308c3b01637c607ce05f52a2fed-Paper.pdf
- [54] F. C. Bauer, G. Lenz, S. Haghghatshoar, and S. Sheik, "Exodus: Stable and efficient training of spiking neural networks," *Frontiers in Neuroscience*, vol. Volume 17 - 2023, 2023. [Online]. Available: <https://www.frontiersin.org/journals/neuroscience/articles/10.3389/fnins.2023.1110444>
- [55] J. Yik, K. V. den Berghe, D. den Blanken, Y. Bouhadjar, M. Fabre, P. Hueber, W. Ke, M. A. Khoei, D. Kleyko, N. Pacik-Nelson, A. Pierro, P. Stratmann, P.-S. V. Sun, G. Tang, S. Wang, B. Zhou, S. H. Ahmed, G. V. Joseph, B. Leto, A. Micheli, A. K. Mishra, G. Lenz, T. Sun, Z. Ahmed, M. Akl, B. Anderson, A. G. Andreou, C. Bartolozzi, A. Basu, P. Bogdan, S. Bohte, S. Buckley, G. Cauwenberghs, E. Chicca, F. Corradi, G. de Croon, A. Danielescu, A. Daram, M. Davies, Y. Demirag, J. Eshraghian, T. Fischer, J. Forest, V. Fra, S. Furber, P. M. Furlong, W. Gilpin, A. Gilra, H. A. Gonzalez, G. Indiveri, S. Joshi, V. Karia, L. Khacef, J. C. Knight, L. Kriener, R. Kubendran, D. Kudithipudi, S.-C. Liu, Y.-H. Liu, H. Ma, R. Manohar, J. M. Margarit-Taulé, C. Mayr, K. Michmizos, D. R. Muir, E. Neftci, T. Nowotny, F. Ottati, A. Ozelikkale, P. Panda, J. Park, M. Payvand, C. Pehle, M. A. Petrovici, C. Posch, A. Renner, Y. Sandamirskaya, C. J. Schaefer, A. van Schaik, J. Schemmel, S. Schmidgall, C. Schuman, J. sun Seo, S. Sheik, S. B. Shrestha, M. Sifalakis, A. Sironi, K. Stewart, M. Stewart, T. C. Stewart, J. Timcheck, N. Tömen, G. Urgese, M. Verhelst, C. M. Vineyard, B. Vogginger, A. Yousefzadeh, F. T. Zohora, C. Frenkel, and V. J. Reddi, "Neurobench: A framework for benchmarking neuromorphic computing algorithms and systems," *Nature Communications*, 2025. [Online]. Available: <https://doi.org/10.1038/s41467-025-56739-4>
- [56] A. Kendall and Y. Gal, "What uncertainties do we need in bayesian deep learning for computer vision?" in *Advances in Neural Information Processing Systems*, I. Guyon, U. V. Luxburg, S. Bengio, H. Wallach, R. Fergus, S. Vishwanathan, and R. Garnett, Eds., vol. 30. Curran Associates, Inc., 2017. [Online]. Available: https://proceedings.neurips.cc/paper_files/paper/2017/file/2650d6089a6d640c5e85b2b88265dc2b-Paper.pdf
- [57] F. Paredes-Valles, Y. Miyatani, and K. Y. W. Scheper, "Realizing fully-integrated, low-power, event-based pupil tracking with neuromorphic hardware," 2025. [Online]. Available: <https://arxiv.org/abs/2511.20175>
- [58] H. Rebecq, R. Ranftl, V. Koltun, and D. Scaramuzza, "High speed and high dynamic range video with an event camera," *IEEE Transactions on Pattern Analysis and Machine Intelligence*, vol. 43, no. 6, pp. 1964–1980, 2021.
- [59] F. Paredes-Valles and G. C. H. E. de Croon, "Back to event basics: Self-supervised learning of image reconstruction for event cameras via photometric constancy," in *Proceedings of the IEEE/CVF Conference on Computer Vision and Pattern Recognition (CVPR)*, June 2021, pp. 3446–3455.
- [60] L. Zhu, X. Wang, Y. Chang, J. Li, T. Huang, and Y. Tian, "Event-based video reconstruction via potential-assisted spiking neural network," in *2022 IEEE/CVF Conference on Computer Vision and Pattern Recognition (CVPR)*, 2022, pp. 3584–3594.
- [61] S. Ahmad, P. Morerio, and A. Del Bue, "Person re-identification without identification via event anonymization," in *Proceedings of the IEEE/CVF International Conference on Computer Vision (ICCV)*, October 2023, pp. 11 132–11 141.
- [62] M. Dampfhofer, T. Mesquida, A. Valentian, and L. Anghel, "Are snns really more energy-efficient than anns? an in-depth hardware-aware study," *IEEE Transactions on Emerging Topics in Computational Intelligence*, vol. 7, no. 3, pp. 731–741, 2023.
- [63] Y. Group, "Neuromorphic computing, memory and sensing 2024," 2024. [Online]. Available: <https://www.yolegroup.com/product/report/neuromorphic-computing-memory-and-sensing-2024/>
- [64] D. Muir and S. Sheik, "The road to commercial success for neuromorphic technologies," *Nature Communications*, vol. 16, 04 2025.